

Freeze-and-release direct optimization method for variational calculations of excited electronic states

Yorick L. A. Schmerwitz,^{*,†,‡} Elli Selenius,[†] and Gianluca Levi^{*,†}

[†]*Science Institute of the University of Iceland, 107 Reykjavík, Iceland*

[‡]*Max-Planck-Institut für Kohlenforschung, 45470 Mülheim an der Ruhr, Germany*

E-mail: schmerwitz@kofo.mpg.de; giale@hi.is

Abstract

Time-independent, orbital-optimized density functional approaches outperform time-dependent density functional theory (TDDFT) in calculations of excited electronic states involving a large rearrangement of the electron density, such as charge transfer excitations. However, optimizing orbitals for excited states remains challenging, as the latter typically correspond to saddle points on the electronic energy surface. A simple and robust strategy for variational orbital optimization of excited states is presented. The approach involves two steps: (1) a constrained energy minimization, where a subset of orbitals changed by the excitation are frozen, followed by (2) a fully unconstrained saddle point optimization. The constrained minimization step makes it possible to identify the electronic degrees of freedom along which the energy needs to be maximized, preventing variational collapse. Both steps of this freeze-and-release strategy are carried out using direct optimization algorithms with a computational scaling comparable to ground state calculations. Numerical tests using a generalized gradient approximation functional are performed on intramolecular charge transfer states of organic molecules

as well as intermolecular charge transfer states of molecular dimers. It is shown that the freeze-and-release direct optimization (FR-DO) approach can successfully converge challenging charge transfer states, overcoming limitations of conventional algorithms based on the maximum overlap method, which either collapse to lower energy, charge-delocalized solutions or fail to converge. While FR-DO requires more iterations on average, the overall increase in computational cost is small. For the NH₃-F₂ dimer, it is found that unlike TDDFT, orbital-optimized calculations reproduce the correct long-range dependency of the energy with respect to the donor-acceptor separation without the need to include exact exchange in the long range.

1 Introduction

Understanding phenomena such as photosynthesis and vision, and developing efficient and sustainable devices for solar energy conversion relies on accurately modeling electronic excitations in large molecular chromophores and photoactive materials. Simulating photoinduced processes, including charge transfer, energy dissipation, and photoisomerization, requires electronic structure methods that are both computationally affordable and can reliably describe states of different electronic character across several molecular geometries. While a host of methods in the contexts of wave function and density functional theory (DFT) have been developed for calculating excited electronic states, combining the efficiency necessary for their employment in large-scale studies with the required accuracy remains a challenge. As a result, conventional excited state methods typically hold low predictive power in simulations of the photoinduced dynamics of the electrons and the positions of the nuclei,^{1,2} calling for the development of efficient methodologies with improved accuracy.

The most favorable balance between efficiency and accuracy is typically achieved in DFT when local or semilocal density functionals are used since then, the expensive evaluation of the exchange interaction is replaced by the efficient calculation of an exchange-and-correlation (XC) functional. Excited states in this framework are most frequently described

by using time-dependent DFT (TDDFT), usually by applying linear-response perturbation theory to the time-dependent Kohn-Sham (KS) equations and using ground state functionals in the adiabatic approximation.³⁻⁵ While competitive to the alternative time-independent formalism regarding efficiency, the approximations used in TDDFT severely limit its applicability in studies of dynamics involving conical intersections^{6,7} and charge transfer excitations which significantly change the electron density.⁸⁻¹¹ These well-known flaws of TDDFT can be alleviated by overcoming the aforementioned approximations, but doing so raises the level of competition in terms of efficiency and non-expert usability of the method so much that accurate and more reliable wave function methods may be a better choice. The inclusion of exact exchange in the functional can improve the TDDFT description of charge transfer excitations,^{9,11-14} but doing so also raises the computational cost and to a degree defeats the point of using DFT in the first place.

Recently, it has been shown that time-independent variational excited state calculations in the framework of DFT yield a more balanced description of ground and excited states than TDDFT when using local and semilocal functionals, with no correlation of the error on the excitation energy with the extent of charge transfer induced by the excitation.¹⁵ This improved performance compared to TDDFT for charge transfer states,^{7,9,16-20} as well as a correct description of a conical intersection of the ethylene molecule²¹ have been demonstrated in other studies as well. Typically referred to as Δ SCF, this method specifically optimizes the orbitals for each excited state by finding solutions to the time-independent KS equations higher in energy than the lowest one corresponding to the ground state. Solutions to these equations are equivalent to stationary points on the energy surface determined by the electronic degrees of freedom.²² Often saddle points,²³⁻²⁷ these stationary points have been difficult to obtain reliably with optimization methods, such as the iterative evaluation and diagonalization of the Fock matrix together with the direct inversion in the iterative subspace (DIIS), classically used for ground state minimizations, which frequently lead to variational collapse to lower-energy solutions other than the desired one or convergence problems. The

probability of variational collapse may be decreased by combining DIIS with the maximum overlap method (MOM)^{7,28} which attempts to conserve a non-aufbau configuration during the minimization to yield SCF-MOM, but this approach is not always successful.^{9,23,29-34} It is now common wisdom that reliable convergence of excited states can only be achieved if the employed solver is specifically designed to converge to saddle points.

Usually, quasi-Newton direct optimization (DO) methods that can update an approximate Hessian with negative eigenvalues are used for this purpose in combination with MOM, an approach termed DO-MOM.^{29,33,34} In order to facilitate convergence toward a saddle point corresponding to a target excited state, the optimization is preconditioned with a diagonal approximation of the initial Hessian containing negative elements. Yet, a recent study has shown that DO-MOM can yield unphysical, charge-delocalized solutions in the case of charge transfer excitation in the 90-degrees-twisted *N*-phenylpyrrole (PP) molecule.²³ An alternative approach is to invert the projection of the gradient along the modes of the electronic Hessian corresponding to the n lowest eigenvalues in order to converge on a saddle point of order n . The resulting direct optimization generalized mode following (DO-GMF) method avoids variational collapse without needing MOM and has been shown to converge challenging charge transfer excitations robustly in the nitrobenzene and PP molecules.²³ However, partial eigendecomposition of the Hessian increases the computational cost, and moreover, the saddle point order of the target solution needs to be estimated ahead of the calculation, which is not straightforward.²³

In the present article, a simple DO strategy that can converge excited states with charge transfer character is presented. The approach involves two optimization steps: (1) A constrained optimization is performed to minimize the energy along all degrees of freedom excluding those where the energy should be maximized, (2) the preconditioner is reevaluated, and a fully unconstrained optimization is carried out. The constrained minimization leads to a partial relaxation of the orbitals in the excited state, improving the estimation of the directions of negative curvature when constructing the preconditioner. In the subsequent

unconstrained optimization, maximization steps are taken in the concave directions, thereby converging on the saddle point corresponding to the target solution. This freeze-and-release direct optimization (FR-DO) approach has similar cost as ground state calculations and is shown here to converge charge transfer excited states of molecules, where DO-MOM calculations collapse to unphysical, charge-delocalized solutions and SCF-MOM computations suffer from convergence problems. The constrained minimization strategy presented here is also found to be useful for estimating the saddle point order of the target excited state solution for calculations using DO-GMF.

2 Methodology

2.1 Direct orbital optimization

In variational electronic structure methods, excited states are obtained as stationary points of an energy functional. These stationary points are generally saddle points on the electronic energy surface, as any variation in the electronic degrees of freedom driving the system toward the ground state—the global minimum—leads to a decrease in energy. In orbital-optimized KS calculations of excited states, the objective is to find a single determinant wave function with a nonaufbau orbital occupation for which the energy functional of the electron density is stationary with respect to unitary variations of the orbitals. Since these stationary points correspond to solutions to the KS equations other than the ground state, a common approach involves solving the KS equations for high energy solutions via eigendecomposition of the KS Hamiltonian matrix, i.e. a simple extension of conventional SCF methods for ground state calculations. However, this approach often suffers from convergence failures and can struggle to maintain the desired nonaufbau occupation during the SCF, even when techniques such as the maximum overlap method are employed, as shown in the present work.

An alternative, more robust approach is direct optimization (DO), where the orbitals are directly optimized by finding a unitary transformation that makes the KS energy sta-

tionary. Given a reference set of M orthonormal molecular orbitals, both occupied and unoccupied, $\boldsymbol{\psi}_0 = (\psi_1^0(\mathbf{r}), \psi_2^0(\mathbf{r}), \dots, \psi_M^0(\mathbf{r}))$, usually chosen as the initial guess orbitals, a new set of orthonormal orbitals $\boldsymbol{\psi} = (\psi_1(\mathbf{r}), \psi_2(\mathbf{r}), \dots, \psi_M(\mathbf{r}))$ is obtained via the unitary transformation

$$\boldsymbol{\psi} = \boldsymbol{\psi}_0 \mathbf{U}. \quad (1)$$

The unitary matrix \mathbf{U} is commonly parametrized as the exponential of an anti-Hermitian matrix $\boldsymbol{\kappa} = -\boldsymbol{\kappa}^\dagger$, such that $\boldsymbol{\psi} = \boldsymbol{\psi}_0 e^{\boldsymbol{\kappa}}$. Therefore, in general, finding the optimal orbitals corresponding to an excited state solution involves making the energy stationary with respect to the elements of $\boldsymbol{\kappa}$ and simultaneously minimizing it with respect to $\boldsymbol{\psi}_0$, which leads to the variational condition

$$\text{stat}_{\boldsymbol{\psi}} E[\boldsymbol{\psi}] = \min_{\boldsymbol{\psi}_0} \text{stat}_{\boldsymbol{\kappa}} E[\boldsymbol{\psi}_0 e^{\boldsymbol{\kappa}}]. \quad (2)$$

In the present work, the molecular orbitals are represented using a linear combination of atomic orbitals (LCAO) basis set, where the initial orbitals $\{\psi_i^0\}$ are expressed as a linear combination of M basis functions

$$\boldsymbol{\psi}_0 = \boldsymbol{\chi} \mathbf{C}_0, \quad (3)$$

where $\boldsymbol{\chi} = (\chi_1(\mathbf{r}), \chi_2(\mathbf{r}), \dots, \chi_M(\mathbf{r}))$ is the vector of basis functions, and \mathbf{C}_0 is the $M \times M$ matrix of expansion coefficients. Since the basis functions $\{\chi_i\}$ are fixed, the variational condition becomes:

$$\text{stat}_{\boldsymbol{\psi}} E[\boldsymbol{\psi}] = \text{stat}_{\boldsymbol{\kappa}} E[\boldsymbol{\chi} \mathbf{C}_0 e^{\boldsymbol{\kappa}}] \quad (4)$$

Thus, in the LCAO basis set, the variational optimization of the orbitals involves finding the elements of $\boldsymbol{\kappa}$ that make the energy stationary, providing a matrix of optimal coefficients.

Anti-Hermitian matrices $\boldsymbol{\kappa}$ form a linear space, which makes it possible to carry out the optimization with gradient-based optimization algorithms. Efficient quasi-Newton methods that propagate a non-positive-definite approximate electronic Hessian have been proposed,^{33,34} and are commonly used. The electronic gradient elements, $\{\partial E / \partial \kappa_{ij}\}$, are com-

puted using the elements of the Hamiltonian matrix in the basis of the optimal orbitals

$$H_{ij} = \sum_{\mu\nu} C_{i\mu}^* H_{\mu\nu} C_{\nu j} \quad (5)$$

with

$$H_{\mu\nu} = \int \chi_{\mu}^*(\mathbf{r}) \hat{\mathbf{h}}_{\text{KS}} \chi_{\nu}(\mathbf{r}) d\mathbf{r}, \quad (6)$$

where $\hat{\mathbf{h}}_{\text{KS}}$ is the KS Hamiltonian operator. The gradients evaluated at each step in the optimization are then used to propagate an approximate inverse electronic Hessian starting from an initial inverse Hessian that acts as a preconditioner for the quasi-Newton step. A common choice for the initial Hessian is a diagonal approximation with elements^{35,36}

$$\frac{\partial^2 E}{\partial \kappa_{ij}^2} \approx 2(\epsilon_i - \epsilon_j)(f_j - f_i) \quad (7)$$

which is easily computed from the eigenvalues, ϵ_i , and occupation numbers, f_i , of the canonical orbitals of the initial guess. Further details on the matrix exponential, gradient evaluation, and propagation of the approximate Hessian can be found in previous works.^{29,33,35}

Recently, an alternative direct optimization approach based on generalized mode following (GMF) has been presented.²³ This method involves determining the eigenvectors of the electronic Hessian corresponding to its lowest n eigenvalues using a numerical partial diagonalization strategy. The components of the electronic gradient along the n modes are then inverted, and a step uphill in energy in the directions parallel to the eigenvectors can be taken using simple minimization methods, thereby converging on a saddle point of order n . The DO-GMF method is more robust than DO methods based on the quasi-Newton step, but requires an accurate estimate of the saddle point order of the target excited state solution.

2.1.1 Direct optimization with constraints

The direct optimization strategy illustrated above can be readily adapted to perform a constrained optimization where a subset of N orbitals is relaxed while the remaining $M - N$ orbitals are kept fixed. Let $\{s_1, s_2, \dots, s_N\}$ be the indices of the N orbitals that are optimized, the elements of the matrix of coefficients after application of the unitary transformation are given by

$$C_{\mu i} = \begin{cases} \sum_{k=1}^N C_{\mu k}^0 [e^{\kappa}]_{ki} & \text{for } i \in \{s_1, s_2, \dots, s_N\} \\ C_{\mu i}^0 & \text{for } i \notin \{s_1, s_2, \dots, s_N\} \end{cases} \quad (8)$$

During the constrained optimization, the gradient can be evaluated using the elements of a reduced $N \times N$ Hamiltonian matrix

$$H'_{kl} = \sum_{\mu\nu} C'_{k\mu}{}^* H_{\mu\nu} C'_{\nu l}, \quad (9)$$

where $k, l \in \{1, 2, \dots, N\}$ are orbital indices in the subspace containing the relaxed orbitals.

2.2 Freeze-and-release direct optimization

The freeze-and-release direct optimization (FR-DO) method is summarized in Algorithm 1. As commonly done, the initial guess for the excited state calculation is formed from ground state orbitals with occupation numbers modified to reflect a desired excitation. For instance, for a HOMO-LUMO excitation, a 90° rotation between the ground state HOMO and LUMO orbitals is performed, effectively swapping their occupation numbers. Here, we focus on single-electron excitations, although the approach can be straightforwardly generalized to handle excitations involving multiple pairs of occupied-unoccupied orbitals.

Next, a constrained optimization is performed where the orbitals involved in the excitation used to prepare the initial guess are kept fixed, constraining all pairwise orbital

Algorithm 1 Freeze-and-Release Direct Optimization

1: Input:

- Ground state orbitals $\{\psi_i^0\}_{i \in \{1, \dots, M\}}$
- Indices of pair of occupied-unoccupied orbitals of target excitation $\{\psi_r^0, \psi_a^0\}$

2: Initial guess excitation

Apply 90° rotation to swap occupation numbers of ψ_r^0 and ψ_a^0
 $\psi_a^0 \leftarrow \psi_r^0$ excitation

3: Constrained subspace optimization

Freeze $\{\psi_r, \psi_a\}$ and optimize remaining orbitals $\{\psi'_k\}_{k \in \{1, \dots, M-2\}} = \{\psi_i^0\}_{i \in \{1, \dots, M\}} \setminus \{\psi_r^0, \psi_a^0\}$
 $\psi' \leftarrow \psi' e^{\kappa'}$

4: Electronic Hessian analysis

Compute approximate Hessian in full space $\{\psi_k\}_{k \in \{1, \dots, M\}} = \{\psi'_k\}_{k \in \{1, \dots, M-2\}} \cup \{\psi_r^0, \psi_a^0\}$
Estimate directions of negative curvature and saddle point order of target excited state

5: Full-space unconstrained optimization

Optimize all M orbitals $\{\psi_k\}_{k \in \{1, \dots, M\}}$
 $\psi \leftarrow \psi e^{\kappa}$

6: Output: Fully optimized excited state orbitals $\{\psi_i\}_{i \in \{1, \dots, M\}}$

rotations involving these orbitals. This step prevents variational collapse to lower-energy solutions while allowing the remaining orbitals to relax. This partial relaxation makes it possible to refine the estimate of the directions of negative curvature, which must be followed to locate the target excited state saddle point. Using the orbitals obtained from the constrained optimization as initial guess, along with the refined approximate Hessian, a subsequent unconstrained optimization is performed in the full orbital space to converge on the saddle point of the target excited state.

This optimization strategy has some similarities with the freeze-and-release method presented by Obermeyer et al.³⁰ in the context of Hartree-Fock-Slater calculations of multiply ionized and highly excited states in molecules. Both approaches involve steps of constrained optimization where some orbitals are frozen, but there are some differences. Firstly, the FR-DO approach uses direct orbital optimization with quasi-Newton algorithms designed to converge on saddle points. The strategy by Obermeyer et al.,³⁰ instead, is based on solving the SCF eigenvalue equation in combinations with MOM. Secondly, in the strategy presented in ref 30, the orbitals kept fixed in the constrained optimization steps are chosen based on the magnitude of the components of the energy gradient. Here, instead, a more bespoke def-

inition of the constraints is adopted, as the fixed orbitals are chosen as the reference orbitals with holes and excited electrons based on excitations within the ground state orbitals. In this way, the degrees of freedom along which the energy should be maximized are initially fixed and the constrained optimization step corresponds to a minimization, which can be performed without the risk of variational collapse.

2.3 Computational settings

Calculations with different orbital-optimized methods are carried out for 27 intramolecular charge transfer excited states of 15 organic molecules, as identified in ref 37 through coupled cluster calculations. The molecular geometries are those obtained in ref 37 by optimizing the vacuum ground state structure at the CCSD(T) or CC3 level. Additionally, orbital-optimized and TD-DFT calculations are performed for intermolecular charge transfer excitations in two molecular dimers, tetrafluoroethylene-ethylene and ammonia-fluorine, at different intermolecular distances. The geometries of the tetrafluoroethylene-ethylene dimer are generated by varying the distance between the two monomers while keeping their internal structures fixed, starting from the dimer optimized in the ground state in vacuum using CC2 in ref 38, while the geometries of the ammonia-fluorine dimer are obtained from a dimer optimized in the ground state in vacuum in ref 39 using a multi-configurational quadratic configuration interaction approach, MC-QCISD/3. The geometries of the two dimers correspond to those used in ref 40, where reference values of excitation energy and charge transfer distance are calculated using equation-of-motion coupled cluster at the CCSD(T) level.

All calculations use the GGA functional PBE and are spin unrestricted.⁴¹ For the orbital-optimized calculations, the frozen core approximation and the projector augmented wave (PAW) formalism⁴² are used. For the systems with intramolecular charge transfer excitations, the valence electrons are represented by an LCAO orbital basis set consisting of primitive Gaussian functions from the aug-cc-pVDZ set⁴³⁻⁴⁵ augmented with a single set of numerical atomic orbitals (referred to as Gaussian basis set + sz).^{46,47} For the systems with

intermolecular charge transfer excitations, cc-pVDZ+sz and cc-pVDZ basis sets are used for the orbital-optimized and TDDFT calculations, respectively. For these calculations, diffuse functions are not included to enable a comparison with the reference EOM-CCSD(T) results of ref 40.

The calculations on the intramolecular charge transfer states are performed with three orbital-optimized methods: (1) the FR-DO approach described in section 2.2, (2) DO-MOM, where direct optimization is used in combination with MOM and no constrained optimization steps are performed, and (3) SCF-MOM, where a conventional DIIS scheme is used together with MOM. For the FR-DO calculations, an L-BFGS algorithm³⁵ with a maximum step size of 0.2 for the constrained optimization step and a limited-memory symmetric rank 1 (L-SR1) algorithm with a maximum step size of 0.1 for the full optimization after releasing the constraints are used. The DO-MOM calculations use L-SR1 with a maximum step size of 0.2. The SCF-MOM calculations are based on direct diagonalization of the KS Hamiltonian matrix with Pulay mixing of the electron density.⁴⁸ Unless otherwise stated, the orbital-optimized calculations are considered converged if a precision of $4 \cdot 10^{-8}$ eV² per valence electron in the squared residual of the KS equations is achieved within 333 iterations (default in the program used for these calculations). In the initial, constrained optimization step of the FR-DO calculations, the orbitals are optimized to a less stringent precision of $4 \cdot 10^{-3}$ eV² per valence electron to optimize efficiency. The results, however, do not change if this first step is converged to $4 \cdot 10^{-8}$ eV² per valence electron.

In the DO-MOM and SCF-MOM calculations, the MOM algorithm of ref. 7 is employed, where at each iteration the occupation numbers are chosen such that the occupied orbitals are those with the largest projections into the occupied space of the initial guess orbitals

$$\omega_i = \sqrt{\sum_{r=1}^N |\Omega_{ri}|^2}, \quad (10)$$

with N being the number of occupied orbitals, and Ω_{ri} being the overlap between occupied

orbital r of the initial guess and orbital i at the current iteration,

$$\Omega_{ri} = \int \psi_r^{0*}(\mathbf{r})\psi_i(\mathbf{r})d\mathbf{r}. \quad (11)$$

All excited states considered in the present work are open-shell singlets, thus the orbital-optimized unrestricted KS calculations provide spin-mixed solutions. For the intramolecular charge transfer states, the focus is on assessing the numerical performance of the FR-DO algorithm in comparison to DO-MOM and SCF-MOM, rather than benchmarking the accuracy of orbital-optimized density functional calculations (for a benchmark of the performance of local and semilocal functional with respect to intramolecular charge transfer excitations, see ref 15). For the intermolecular charge transfer states, for which a comparison with reference coupled cluster calculations is carried out, the effect of spin mixing on the energy has been shown to be negligible,⁴⁰ since spin-mixed and triplet solutions become degenerate for long distances between donor and acceptor. Therefore, in all calculations presented here, no spin purification of the energy⁴⁹ is applied.

Apart from the value of excitation energy, orbital-optimized solutions are characterized by computing a charge transfer distance according to the metric introduced by Le Bahers et al.:⁵⁰

$$d^{\text{CT}} = \frac{|\int \Delta\rho(\mathbf{r})\mathbf{r} d\mathbf{r}|}{q^{\text{CT}}}, \quad (12)$$

where $\Delta\rho(\mathbf{r})$ is the electron density difference between the excited and ground states, and q^{CT} is the charge transferred in the excitation evaluated as the integral of the positive part of $\Delta\rho(\mathbf{r})$.

The orbital-optimized calculations are carried out with the Grid-based Projector Augmented Wave (GPAW) software,^{48,51,52} where the FR-DO method is implemented. For the TD-DFT calculations, version 5.0.4 of the ORCA software^{53,54} is used.

3 Results

3.1 Numerical tests

3.1.1 Charge transfer excited state of twisted *N*-Phenylpyrrole

It has previously been shown that charge transfer excited states of the *N*-Phenylpyrrole (PP) molecule are challenging to obtain within orbital optimized density functional calculations.²³ Here, the performance of the FR-DO approach presented in sec. 2.2 is assessed with respect to the A_1 LUMO+1 \leftarrow HOMO charge transfer excitation in twisted PP.

As shown in Figure 1, a calculation of the spin-mixed solution for the A_1 excited state of PP is initialized by promoting an electron from the ground state HOMO localized on the pyrrole group (π_{py}) to the ground state LUMO+1 localized on the phenyl group (π_{ph}^*). Figure 2 shows the convergence of the energy in DO-MOM and FR-DO using the PBE functional and the aug-cc-pVDZ+sz basis set started from the same initial guess. The DO-MOM calculation converges after 34 iterations to a solution with an excitation energy of 4.61 eV, while FR-DO converges in only 27 iterations to a higher-energy solution with an excitation energy of 5.56 eV, much closer to the theoretical best estimate of 5.65 eV.³⁷ The solution obtained with FR-DO has larger dipole moment and charge transfer distance $d_{\text{DO}}^{\text{CT}}$ (9.36 D and 2.42 Å) compared to the solution obtained with DO-MOM (3.33 D and 2.06 Å). The value of $d_{\text{DO}}^{\text{CT}}$ of 2.42 Å is in good agreement with the charge transfer distance obtained from the relaxed density of TD-DFT calculations with the range-separated CAM-B3LYP functional and the cc-pVTZ basis set in ref 37 (2.38 Å). Clearly, the solution that best describes the target charge transfer excited state is the one obtained with FR-DO, while DO-MOM collapses to a solution where the transferred charge is too delocalized.

In Figure 1, the canonical orbitals of the charge-localized and charge-delocalized solutions are visualized together with their occupations. At the initial guess, the electron hole created by the excitation is localized on the pyrrole group (π_{py} orbital). However, in the solution obtained with DO-MOM, the hole is delocalized over the entire molecule and is nearly

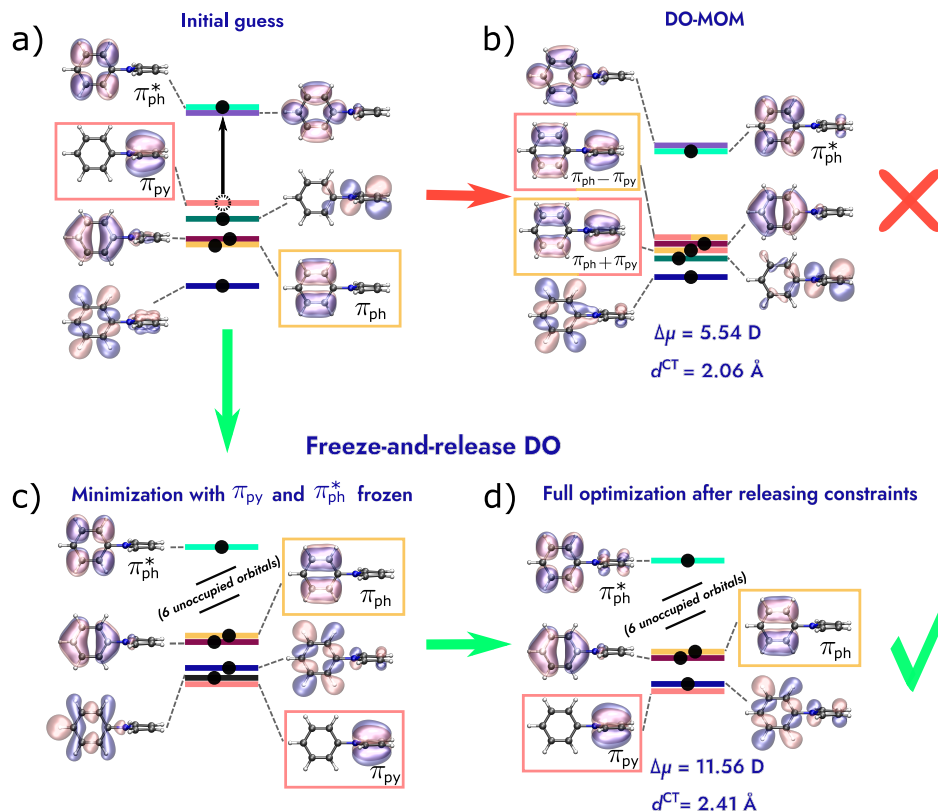


Figure 1: DO-MOM vs. FR-DO solutions of the spin-mixed A_1 charge transfer excited state of the twisted *N*-Phenylpyrrole molecule obtained with PBE/aug-cc-pVDZ+sz. (a) The initial guess is formed from the ground state orbitals by choosing the occupations according to a $\pi_{ph}^* \leftarrow \pi_{py}$ excitation (HOMO to LUMO+1). (b) DO-MOM converges to a solution corresponding to a 2nd-order saddle point with small dipole moment and charge transfer distance, where the π_{py} hole and a π_{ph} occupied orbital are mixed by $\sim 45^\circ$. (c) The first step of constrained minimization in FR-DO prevents π_{py} and π_{ph} from mixing. (d) When the constraints are released, the calculation converges to a 10th-order saddle point with larger dipole moment and charge transfer distance in better agreement with the results of higher-level calculations.³⁷ The orbitals are visualized for isosurface values of ± 0.08 Å⁻³. Some of the orbitals are omitted for clarity.

degenerate with an equally delocalized occupied orbital, leading to a reduced charge transfer. The pair of delocalized occupied-unoccupied orbitals arise from approximately 45° mixing between the unoccupied π_{py} orbital and a lower-energy occupied orbital localized on the phenyl group, π_{ph} , as demonstrated in Figure 3, where the orbital projections used by MOM are shown for each iteration. This is confirmed in Figure 4, which shows a scan of the energy along the degree of freedom corresponding to the rotation between the π_{ph} and π_{py} orbitals, $\kappa_{\pi_{ph}\pi_{py}}$. Along this orbital rotation, the energy has a minimum where the π_{ph} and

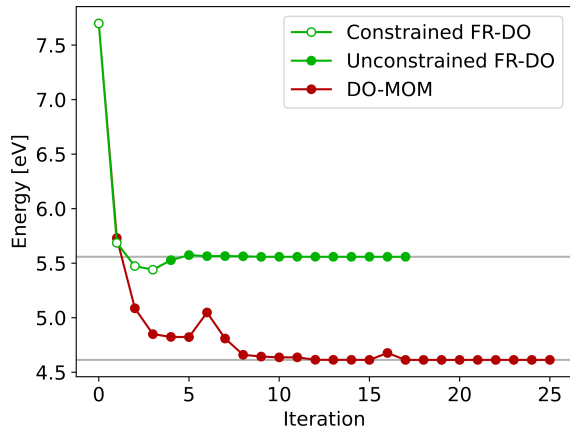


Figure 2: Convergence of the excitation energy in DO-MOM and FR-DO calculations of the spin-mixed A_1 charge transfer excited state of twisted *N*-Phenylpyrrole using PBE/aug-cc-pVDZ+sz. FR-DO converges to a charge-localized solution with excitation energy (5.56 eV) close to the theoretical best estimate (5.86 eV), while DO-MOM collapses to a lower-energy (4.61 eV), charge-delocalized solution (see also Figure 1).

π_{py} orbitals are highly mixed. FR-DO avoids collapse along $\kappa_{\pi_{\text{ph}}\pi_{\text{py}}}$, giving a solution where π_{ph} and π_{py} are still localized on the phenyl and pyrrole groups, respectively, corresponding to a maximum along $\kappa_{\pi_{\text{ph}}\pi_{\text{py}}}$.

To understand why DO-MOM converges to a lower-energy solution with unphysical charge delocalization while FR-DO avoids this collapse, a closer look at the preconditioning procedure of the quasi-Newton algorithm needs to be taken. The preconditioner for the DO-MOM calculation evaluated as the inverse of a diagonal approximation to the electronic Hessian according to eq 7 using the energy of the initial guess orbitals has two negative elements, since there are two unoccupied orbitals below one occupied orbital at the initial guess (see Figure 1). However, the component of the preconditioner along $\kappa_{\pi_{\text{ph}}\pi_{\text{py}}}$ is positive because the unoccupied orbital π_{py} has higher energy than the occupied orbital π_{ph} . As a result, DO-MOM takes a step toward the direction of the negative of the gradient along $\kappa_{\pi_{\text{ph}}\pi_{\text{py}}}$, leaving the concave region of the energy surface and going downhill toward the stationary point where the π_{ph} and π_{py} orbitals are mixed. This solution is a 2nd-order saddle point, consistent with the number of negative elements of the preconditioner. Figure 3 shows the orbital projections that MOM uses as weights according to eq 10. Initially, the (occu-

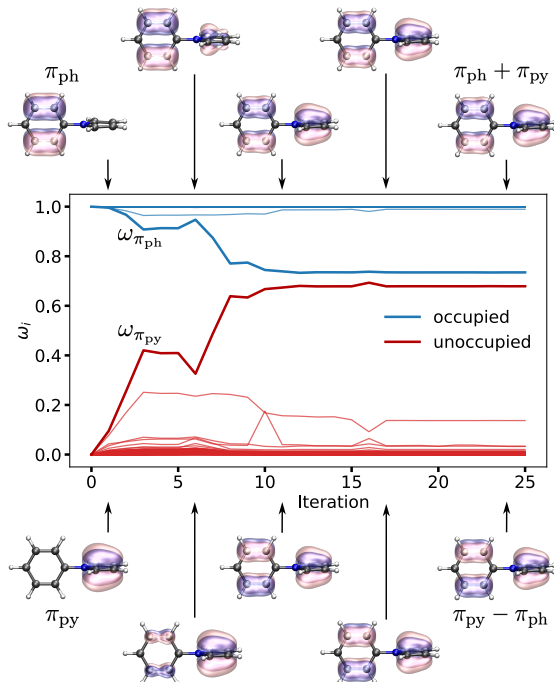


Figure 3: Orbital projections according to eq 10 used as weights to choose the occupation numbers in a DO-MOM calculation of the spin-mixed solution of the A_1 LUMO+1 \leftarrow HOMO charge transfer excited state in the twisted *N*-Phenylpyrrole molecule with PBE/aug-cc-pVDZ. $\omega_{\pi_{py}}$ and $\omega_{\pi_{ph}}$ are the projections for the (occupied) π_{ph} and (unoccupied) π_{py} orbitals, respectively. These orbitals are visualized for selected iterations with isosurface values of $\pm 0.1 \text{ \AA}^{-3}$, showing the mixing between the orbitals.

occupied) π_{ph} and (unoccupied) π_{py} orbitals are localized on the phenyl and pyrrole parts of the molecule and their projections according to eq 10 are 1 and 0, respectively. As the calculation collapses to a solution corresponding to a minimum along the rotation angle $\kappa_{\pi_{ph}\pi_{py}}$ mixing π_{ph} and π_{py} (see Figure 4), the projections approach $1/\sqrt{2} \approx 0.7$, corresponding to an absolute mixing of $\sim 45^\circ$. MOM is unable to prevent the variational collapse as there are no orbitals with larger overlaps with the initially localized π_{ph} orbital among the manifold of unoccupied orbitals. In the first step of FR-DO, the π_{ph} and π_{py} orbitals are frozen, so there is no possibility of leaving the concave region of the energy surface along $\kappa_{\pi_{ph}\pi_{py}}$.

The constrained minimization induces a reordering of the orbitals by stabilizing the orbitals localized on the phenyl group and destabilizing the orbitals localized on the pyrrole group. As a result, the preconditioner evaluated using the partially relaxed orbitals has

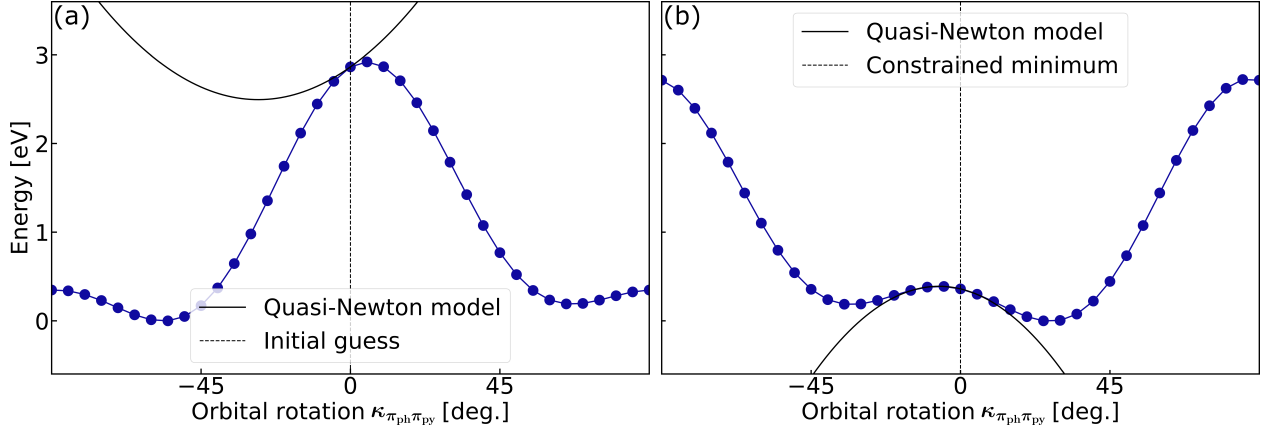


Figure 4: Electronic energy of twisted *N*-Phenylpyrrole as a function of the rotation angle $\kappa_{\pi_{\text{ph}}\pi_{\text{py}}}$ mixing the occupied π_{ph} and unoccupied π_{py} orbitals (see Figure 1) using PBE/aug-cc-pVDZ+sz. The minima of the energy along $\kappa_{\pi_{\text{ph}}\pi_{\text{py}}}$ correspond to unphysical, charge-delocalized solutions, while the target charge-localized solution corresponds to the maximum closest to 0° rotation. The black continuous curves represent the quadratic model used by the quasi-Newton algorithm employed in the calculations based on the energy gradient and Hessian approximation (eq 7) at the initial guess. In a DO-MOM calculation (a), the quadratic model incorrectly gives a positive curvature because the Hessian approximation underestimates the directions of negative curvature, and the quasi-Newton step is away from the target saddle point. After constrained minimization in FR-DO (b), the model predicts the correct negative curvature and the step is toward the saddle point.

12 negative elements, two being close to zero. One of the negative components of the preconditioner is along $\kappa_{\pi_{\text{ph}}\pi_{\text{py}}}$ because the occupied π_{ph} orbital lies higher in energy than the π_{py} hole after the constrained minimization (see Figure 1). Therefore, when the constraints are released, a step is taken in the direction of the positive gradient along $\kappa_{\pi_{\text{ph}}\pi_{\text{py}}}$, thereby converging on the saddle point corresponding to the target charge-localized solution. The saddle point order of this solution is 10, which is consistent with the number of large negative elements of the diagonal approximate Hessian evaluated after the constrained minimization. The saddle point orders of all solutions are shown in Table S2.

3.1.2 Saddle point order of target excited states

The constrained minimization step of FR-DO provides an improved estimate of the degrees of freedom along which the energy needs to be maximized preventing collapse to lower-energy solutions for a calculation of a charge transfer excited state of the twisted PP molecule.

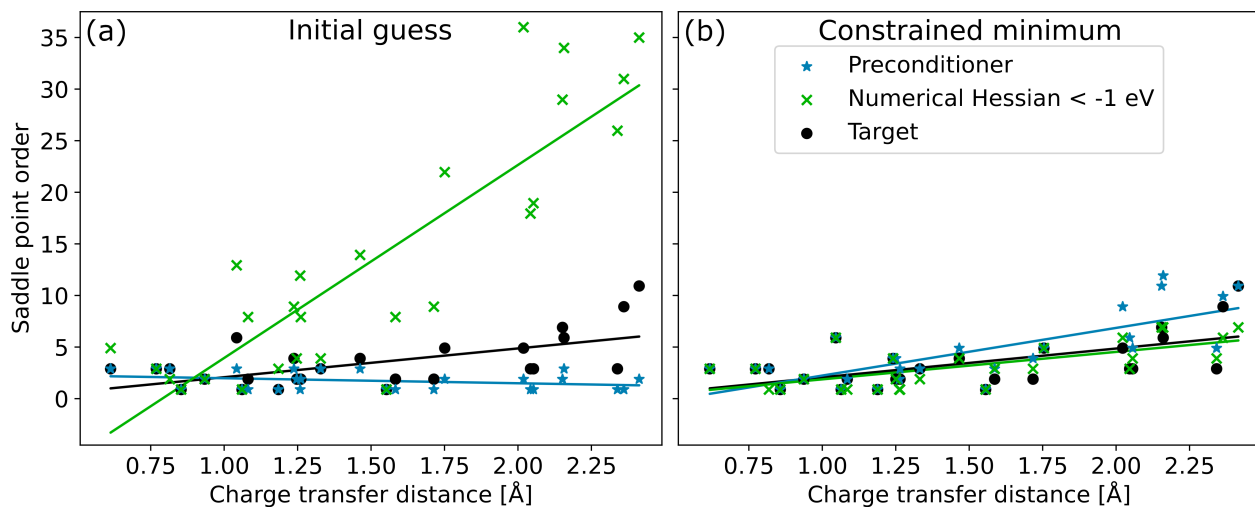


Figure 5: Comparisons of estimated saddle point orders using PBE/aug-cc-pVDZ of all excited states in the set of intramolecular charge transfer states predicted from the number of negative elements of the preconditioner (blue stars) and the number of negative eigenvalues of the numerical electronic Hessian smaller than -1 eV (green crosses), and the true saddle point orders of the converged solutions (black circles) depending on the charge transfer distance of the converged solution. The lines show linear regressions. At the initial guess (a), the preconditioner tends to underestimate the saddle point order, while the numerical Hessian generally overestimates it. Constrained minimization (b) improves the estimates, with the preconditioner slightly overestimating the true saddle point orders and the numerical Hessian agreeing with them with an average deviation of 0.56 (see Table S2).

The question arises as to what extent constrained minimization can be used to estimate the saddle point order of a target excited state solution. This is an important consideration in, e.g., calculations with the direct optimization generalized mode following method, DO-GMF, presented in ref 23, which requires the saddle point order of the excited state as input for a calculation.

Figure 5 shows the saddle point order estimated at the initial guess made of ground state orbitals with changed occupations and at the partially relaxed solution obtained after constrained minimization for multiple charge transfer excited states in organic molecules from Loos’ benchmark set,³⁷ including the A_1 state of twisted PP analyzed in the previous section.

The saddle point order is estimated as the number of negative eigenvalues of the electronic Hessian evaluated numerically using a Davidson algorithm²³ as well as the number of negative elements of an analytical diagonal approximation to the Hessian, the inverse of the preconditioner of eq 7. The saddle point order of the final solution is also shown in Table S2. At the initial guess made of ground state orbitals, the numerical and approximate analytic Hessians overestimate and underestimate the saddle point order, respectively. The deviation is larger the bigger the charge transfer distance. For the A_1 state of PP, which is the state with biggest charge transfer distance, the numerical Hessian gives 32 too many negative eigenvalues, while the preconditioner gives 8 too few negative eigenvalues. The constrained minimization generally leads to a considerable improvement in the estimation of the saddle point order, with the numerical and approximate analytic Hessians being in agreement with each other. In some cases, the numerical Hessian and the preconditioner overestimate the number of negative eigenvalues, with the largest deviation being equal to 3 (A_2 state of twisted DMABN). However, in those cases the magnitude of some of the negative eigenvalues is small. Table S2 reports also the saddle point order estimated at the constrained solution by considering only negative eigenvalues with absolute value bigger than 1 eV. In the case of the A_1 state of twisted DMABN, excluding the small eigenvalues gives a saddle point order

in agreement with the saddle point order of the final solution.

3.2 Performance of the methods on intramolecular charge transfer states

The performance on each excitation in the benchmark set of the SCF-MOM, DO-MOM, and FR-DO methods in terms of optimization iterations until convergence is reached is illustrated in Figure S1. The numbers of convergence failures and variational collapses as well as the average and maximum numbers of iterations taken are gathered in Table 1. While SCF-MOM fails to converge in 2 cases, it shows no variational collapses in the cases it does converge. DO-MOM, on the other hand, converges in all cases, but shows 4 variational collapses, the reasons for which have already been discussed in sec. 3.1.1. Excluding variational collapses, DO-MOM takes 11.7 iterations on average to reach convergence. If a calculation suffers from variational collapse, convergence takes longer leading to an increase of the average number of iterations to 12.8 if variational collapse is taken into account. In this case, DO-MOM still on average takes 6.4 iterations less than SCF-MOM. FR-DO takes 5.9 iterations more than DO-MOM on average, but converges to the desired solution in all cases. The average performance of FR-DO is slightly better than that of SCF-MOM. As can be seen in Figure S1, including all convergence problems and variational collapses encountered in the entire set, the excited states of the PP and benzonitrile molecules are the most challenging for the three methods. Particularly in these cases, DO-MOM tends to outperform the other methods in terms of iteration count, but with a high risk of variational collapse, whereas FR-DO converges to the target solution.

3.3 Intermolecular charge transfer states

Intermolecular charge transfer excited states provide an excellent way of analyzing the dependence of the accuracy of a method on the charge transfer distance since the separation be-

Table 1: Number of convergence failures (more than 333 iterations) and variational collapses, average number (avg. no.) and maximum number (max. no.) of iterations of FR-DO, DO-MOM, and SCF-MOM for the set of intramolecular charge transfer states.

	FR-DO	DO-MOM	SCF-MOM
Convergence failures	0	0	2
Variational collapses	0	4	0
Avg. no. of iterations ^a	17.6	11.7	19.2
Max. no. of iterations ^a	55	18	139
Avg. no. of iterations ^b	17.6	12.8	19.2
Max. no. of iterations ^b	55	25	139

^a Excluding unconverged and variationally collapsed calculations

^b Excluding unconverged calculations

tween the donor and acceptor of the charge transfer can be changed systematically by controlling the distance between the molecular fragments. Here, we consider the tetrafluoroethene-ethene dimer and the ammonia-fluorine dimer. The excitation energy values depending on the distance between the molecular fragments obtained with FR-DO, DO-MOM, and SCF-MOM at the PBE/cc-pVDZ level of theory and published results for EOM-CCSD(T)⁴⁰ are collected in Table 2. The dimer separation is defined as the shortest distance between atoms of the two fragments.

Table 2: Excitation energy values (in eV) obtained with FR-DO, DO-MOM, and SCF-MOM for the intermolecular charge transfer excitations considered and published results for EOM-CCSD(T).⁴⁰

Molecule	Dimer separation [Å]	EOM-CCSD(T)	FR-DO	DO-MOM	SCF-MOM
Ammonia-Fluorine	3.5	7.75	8.33	6.81	8.33
Ammonia-Fluorine	4.25	8.19	8.77	–	8.77
Ammonia-Fluorine	5	8.53	9.07	–	9.07
Ammonia-Fluorine	8	9.34	9.75	9.75	9.75
Ammonia-Fluorine	10	9.63	9.95	9.95	9.95
Tetrafluoroethylene-ethylene	3.5	8.19	8.10	5.05	8.10
Tetrafluoroethylene-ethylene	4.25	9.68	8.90	8.90	8.90
Tetrafluoroethylene-ethylene	5	9.94	9.61	–	9.65

3.3.1 Tetrafluoroethene-ethene dimer

The charge transfer excitation in the tetrafluoroethene-ethene dimer occurs from the HOMO of the ethene molecule to the LUMO of the tetrafluoroethene molecule. For a dimer distance of 3.5 Å, DO-MOM, again, shows a variational collapse leading to a charge-delocalized solution more than 3 eV lower in energy than the solutions obtained with FR-DO and SCF-MOM. The molecular orbitals (MOs) of this charge-delocalized solution and the solution

with the expected charge transfer character obtained with FR-DO are illustrated in Figure 6. While for FR-DO, all MOs are localized on either of the two molecular fragments, several MOs are significantly delocalized over both fragments in the solution obtained with DO-MOM, resulting in an artificial delocalization of the charge supposed to be transferred in the excitation. The FR-DO solution corresponds to a 9th-order saddle point on the electronic energy surface, whereas the collapsed DO-MOM solution corresponds to a 1st-order saddle point. At a dimer distance of 4.25 Å, all methods converge to the same charge-localized solution. DO-MOM fails to converge at a dimer distance of 5 Å, while FR-DO and SCF-MOM converge to numerically slightly different but qualitatively similar solutions.

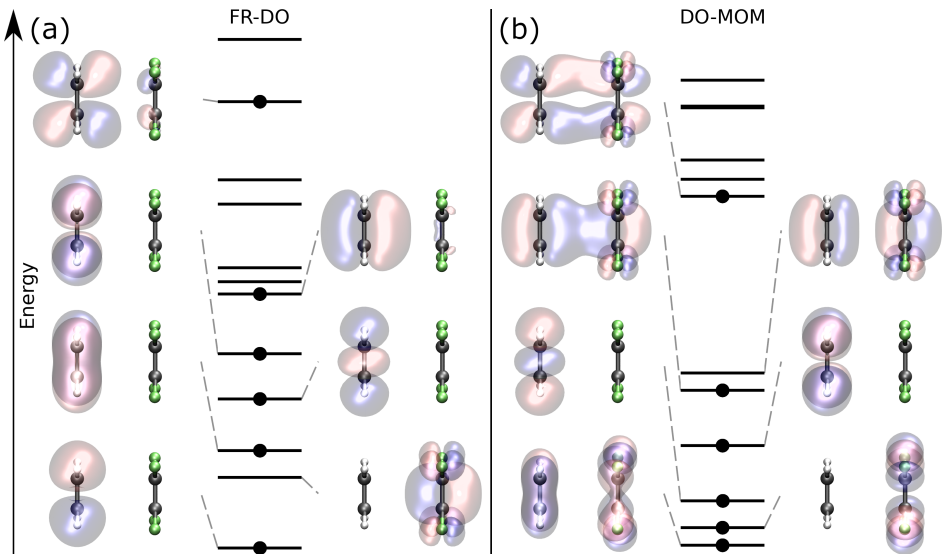


Figure 6: MOs of an intermolecular charge transfer excited state of the tetrafluoroethene dimer obtained with PBE/cc-pVDZ for a dimer separation of 3.5 Å with (a) FR-DO and (b) DO-MOM. The FR-DO calculation converges to the desired solution, which corresponds to a 9th-order saddle point and shows no significant mixing between orbitals localized on different fragments. The DO-MOM calculation collapses to a 1st-order saddle point with clear mixing between orbitals localized on different fragments. The orbitals are visualized with isosurface values of $\pm 0.08 \text{ \AA}^{-3}$.

3.3.2 Ammonia-fluorine dimer

In the ammonia-fluorine dimer, the charge transfer excitation occurs from the HOMO of the ammonia molecule to the LUMO of the fluorine molecule, as illustrated in Figure S3. While

DO-MOM shows a variational collapse at a dimer distance of 3.5 Å and does not converge within 333 iterations for distances of 4.25 Å and 5 Å, all three methods, DO-MOM, FR-DO, and SCF-MOM, converge to the same solution for separations of 8 Å and 10 Å. FR-DO and SCF-MOM always converge to the same solution, with FR-DO converging slightly faster (1-2 iterations) than SCF-MOM, similarly to the situation for the benchmark set of intramolecular charge transfer excitations. Figure 7 shows comparisons of the shapes of the excitation energy curves and the charge transfer distances with respect to the dimer distance obtained with FR-DO and TDDFT with the PBE functional and the aug-cc-pVDZ basis set to reference values evaluated with the EOM-CCSD(T) method taken from ref. 40. While TDDFT with this semilocal functional demonstrates the well-known^{11,55-57} qualitatively incorrect shape of the excitation energy curve, FR-DO agrees with the EOM-CCSD(T) quite well. The TDDFT charge transfer distances make use of the Z vector method. The charge transfer distances of all methods agree very well with the exception of the TDDFT result for a dimer distance of 3.5 Å.

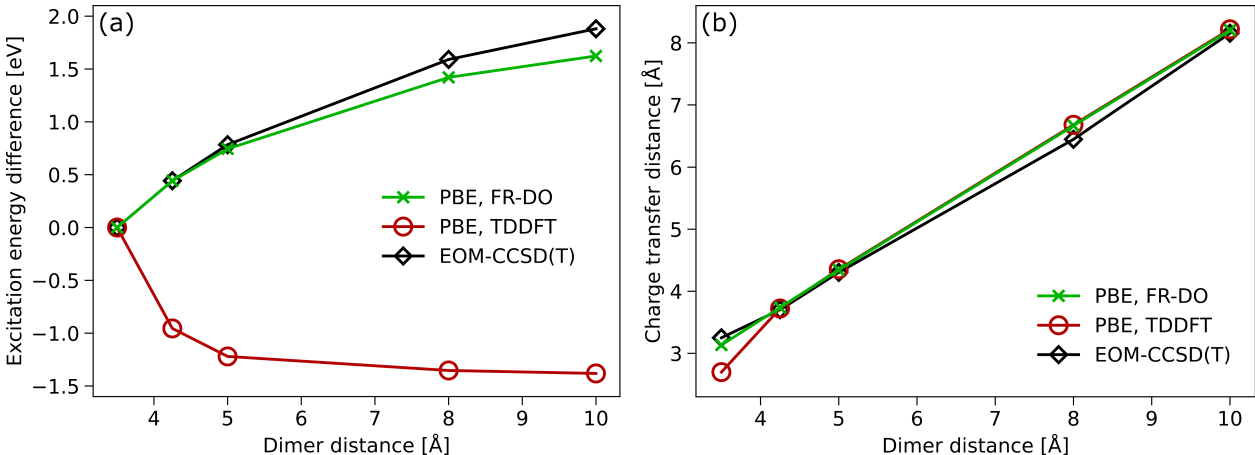


Figure 7: Comparisons of (a) the excitation energy and (b) the charge transfer distance of the ammonia-fluorine dimer depending on the distance between the molecular fragments obtained with FR-DO (green crosses) and TDDFT (red circles) using PBE/aug-cc-pVDZ, and taken from published EOM-CCSD(T) calculations⁴⁰ (black squares). The TDDFT charge transfer distance uses the Z vector method. The TDDFT excitation energy curve shows the qualitatively incorrect trend compared to EOM-CCSD(T), while FR-DO agrees with the higher level of theory. With the exception of the TDDFT result for a dimer distance of 3.5 Å, the charge transfer distances agree well.

4 Discussion and conclusions

While the ground state in density functional theory can be targeted as the stationary solution with lowest energy according to a minimum energy principle, it is hard to predict the saddle point order of the solution that best represents the target excited state in time-independent variational excited state calculations. Here, it is found that for charge transfer excitations in organic molecules, the appropriate charge-localized solution corresponds to a higher-order saddle point than unphysical, charge-delocalized solutions. Routine SCF calculations are typically geared toward minimization and can lead to collapse to lower-energy solutions with lower saddle point order.⁹ Direct optimization of saddle points on the electronic energy surface has proven more robust than conventional SCF algorithms.^{21,29,33} However, DO approaches rely on the estimation of the electronic degrees of freedoms along which the energy should be maximized. For excitations with weak charge transfer character, a preconditioner consisting of the inverse of an approximate diagonal form of the electronic Hessian at the initial guess using the ground state orbitals usually provides the required accuracy, as shown in section 3.1.2. When the charge transfer character is strong, however, this preconditioner tends to underestimate the number of directions of negative curvature, and DO-MOM calculations can collapse to spurious lower-energy, charge-delocalized solutions, even if the initial guess is closer to the target saddle point than the undesired solution. It is important to note that MOM by construction is unable to prevent variational collapse for mixing of the initial orbitals by less than 45° , as in the case of the A_1 state of twisted PP, as discussed in section 3.1.1. An alternative DO method based on generalized mode following (DO-GMF) has proven more robust than DO-MOM,²³ but it requires the saddle point order of the target solution as input. Numerical eigendecomposition of the Hessian at the initial guess based on ground state orbitals does not provide an accurate enough estimate of the target saddle point order for charge transfer excitations, as it tends to overestimate the saddle point order significantly. These issues stem from the fact that charge transfer leads to a large rearrangement of the orbitals upon relaxation in the excited state, and thus the energy surface at the

initial guess has a curvature significantly different from that at the final solution.

A first optimization step where the orbitals with holes and excited electrons are frozen allows the orbitals not directly involved in the excitation to adjust to the effect of the charge transfer, providing an improved estimation of the directions of negative curvature for a subsequent, fully unconstrained optimization. The resulting FR-DO strategy proves highly effective in converging to high-order saddle points corresponding to charge transfer excited states, as demonstrated here. The constrained optimization can also be combined with the DO-GMF method, as the partially relaxed orbitals provide an improved excited state saddle point order estimate. An additional benefit is that the cost ahead of a DO-GMF calculation can be kept low by avoiding the computationally expensive eigendecomposition of the Hessian, as the analytical diagonal approximation to the Hessian at the solution of the constrained optimization is found to have comparable accuracy, unless the charge transfer character of the excitation is very strong, as discussed in section 3.1.2. For some of the charge transfer states analyzed, the saddle point order can still be overestimated by up to three. Therefore, when using DO-GMF, it is advisable to carry out a few calculations for saddle point orders around the one estimated from the constrained solution to ensure that the target charge-localized excited state is found. This process can be automated by carrying out the saddle point searches in parallel and choosing the target solution as the one with the largest charge transfer distance.

Acknowledgement

This work was funded by the Icelandic Research Fund (grants nos. 217734, 217751 and 239678). Y.L.A.S. acknowledges support by the Max Planck Society. The calculations were carried out at the Icelandic High Performance Computing Center (IHPC) facility. The authors thank Nicola Bogo and Christopher J. Stein for providing the reference values of excitation energy and charge-transfer distance, as well as geometries, of the molecular dimers.

The authors also thank Alec Elías Sigurdarson for useful discussions and comments on the manuscript.

Supporting Information Available

Excitation energies and charge transfer distances with FR-DO, DO-MOM, and SCF-MOM; estimation of the saddle point order at the initial guess, the constrained solution, and the final solution; number of iterations taken by FR-DO, DO-MOM, and SCF-MOM; comparison of the excitation energy as a function of separation for ammonia-fluorine with FR-DO, DO-MOM, and the theoretical best estimate.

References

- (1) Mukherjee, S.; Mattos, R. S.; Toldo, J. M.; Lischka, H.; Barbatti, M. Prediction Challenge: Simulating Rydberg photoexcited cyclobutanone with surface hopping dynamics based on different electronic structure methods. *Journal of Chemical Physics* **2024**, *160*, 154306.
- (2) Janoš, J.; Slavíček, P. What Controls the Quality of Photodynamical Simulations? Electronic Structure Versus Nonadiabatic Algorithm. *Journal of Chemical Theory and Computation* **2023**, *19*, 8273–8284.
- (3) Casida, M. E. *Recent Advances In Density Functional Methods: (Part I)*; World Scientific, 1995; pp 155–192.
- (4) Runge, E.; Gross, E. K. U. Density-functional theory for time-dependent systems. *Phys. Rev. Lett.* **1984**, *52*, 997–1000.
- (5) Hohenberg, P.; Kohn, W. Inhomogeneous electron gas. *Physical review* **1964**, *136*, B864.

- (6) Levine, B. G.; Ko, C.; Quenneville, J.; Martínez, T. J. Conical intersections and double excitations in time-dependent density functional theory. *Molecular Physics* **2006**, *104*, 1039–1051.
- (7) Barca, G. M.; Gilbert, A. T.; Gill, P. M. Simple models for difficult electronic excitations. *J. Chem. Theory Comput.* **2018**, *14*, 1501–1509.
- (8) Mester, D.; Kállay, M. Charge-Transfer Excitations within Density Functional Theory: How Accurate Are the Most Recommended Approaches? *J. Chem. Theory Comput.* **2022**, *18*, 1646–1662.
- (9) Hait, D.; Head-Gordon, M. Orbital optimized density functional theory for electronic excited states. *The J. Phys. Chem. Lett.* **2021**, *12*, 4517–4529.
- (10) Dev, P.; Agrawal, S.; English, N. J. Determining the appropriate exchange-correlation functional for time-dependent density functional theory studies of charge-transfer excitations in organic dyes. *J. Chem. Phys.* **2012**, *136*.
- (11) Ghosh, S.; Sonnenberger, A. L.; Hoyer, C. E.; Truhlar, D. G.; Gagliardi, L. Multiconfiguration Pair-Density Functional Theory Outperforms Kohn-Sham Density Functional Theory and Multireference Perturbation Theory for Ground-State and Excited-State Charge Transfer. *Journal of Chemical Theory and Computation* **2015**, *11*, 3643–3649.
- (12) Liang, J.; Feng, X.; Hait, D.; Head-Gordon, M. Revisiting the performance of time-dependent density functional theory for electronic excitations: Assessment of 43 popular and recently developed functionals from rungs one to four. *J. Chem. Theory Comput.* **2022**,
- (13) Shee, J.; Head-Gordon, M. Predicting excitation energies of twisted intramolecular charge-transfer states with the time-dependent density functional theory: Comparison with experimental measurements in the gas phase and solvents ranging from hexanes to acetonitrile. *J. Chem. Theory Comput.* **2020**, *16*, 6244–6255.

- (14) Kronik, L.; Stein, T.; Refaely-Abramson, S.; Baer, R. Excitation gaps of finite-sized systems from optimally tuned range-separated hybrid functionals. *J. Chem. Theory Comput.* **2012**, *8*, 1515–1531.
- (15) Selenius, E.; Sigurdarson, A. E.; Schmerwitz, Y. L.; Levi, G. Orbital-Optimized Versus Time-Dependent Density Functional Calculations of Intramolecular Charge Transfer Excited States. *J. Chem. Theory Comput.* **2024**, *20*, 3809–3822.
- (16) Briggs, E. A.; Besley, N. A. Density functional theory based analysis of photoinduced electron transfer in a triazacryptand based K⁺ sensor. *J. Phys. Chem. A* **2015**, *119*, 2902–2907.
- (17) Kumar, C.; Lubner, S. Robust Δ SCF calculations with direct energy functional minimization methods and STEP for molecules and materials. *J. Chem. Phys.* **2022**, *156*, 154104.
- (18) Hait, D.; Zhu, T.; McMahon, D. P.; Van Voorhis, T. Prediction of excited-state energies and singlet–triplet gaps of charge-transfer states using a restricted open-shell Kohn–Sham approach. *J. Chem. Theory Comput.* **2016**, *12*, 3353–3359.
- (19) Zhekova, H. R.; Seth, M.; Ziegler, T. A perspective on the relative merits of time-dependent and time-independent density functional theory in studies of the electron spectra due to transition metal complexes. An illustration through applications to copper tetrachloride and plastocyanin. *Int. J. Quantum Chem.* **2014**, *114*, 1019–1029.
- (20) Himmetoglu, B.; Marchenko, A.; Dabo, I.; Cococcioni, M. Role of electronic localization in the phosphorescence of iridium sensitizing dyes. *J. Chem. Phys.* **2012**, *137*, 154309.
- (21) Schmerwitz, Y. L.; Ivanov, A. V.; Jónsson, E. Ö.; Jónsson, H.; Levi, G. Variational Density Functional Calculations of Excited States: Conical Intersection and Avoided Crossing in Ethylene Bond Twisting. *The J. Phys. Chem. Lett.* **2022**, *13*, 3990–3999.

- (22) Helgaker, T.; Jørgensen, P.; Olsen, J. *Molecular Electronic-Structure Theory*; John Wiley & Sons, Ltd, 2014; Chapter 4, pp 107–141.
- (23) Schmerwitz, Y. L. A.; Levi, G.; Jónsson, H. Calculations of Excited Electronic States by Converging on Saddle Points Using Generalized Mode Following. *J. Chem. Theory Comput.* **2023**, *19*, 3634–3651.
- (24) Marie, A.; Burton, H. G. A. Excited states, symmetry breaking, and unphysical solutions in state-specific CASSCF theory. *Journal of Physical Chemistry A* **2023**,
- (25) Burton, H. G. Energy Landscape of State-Specific Electronic Structure Theory. *J. Chem. Theory Comput.* **2022**, *18*, 1512–1526.
- (26) Kossoski, F.; Loos, P.-F. State-Specific Configuration Interaction for Excited States. *J. Chem. Theory Comput.* **2023**, *19*, 2258–2269.
- (27) Perdew, J. P.; Levy, M. Extrema of the density functional for the energy: Excited states from the ground-state theory. *Phys. Rev. B* **1985**, *31*, 6264–6272.
- (28) Gilbert, A. T.; Besley, N. A.; Gill, P. M. Self-consistent field calculations of excited states using the maximum overlap method (MOM). *J. Phys. Chem. A* **2008**, *112*, 13164–13171.
- (29) Ivanov, A. V.; Levi, G.; Jónsson, E. Ö.; Jónsson, H. Method for Calculating Excited Electronic States Using Density Functionals and Direct Orbital Optimization with Real Space Grid or Plane-Wave Basis Set. *J. Chem. Theory Comput.* **2021**, *17*, 5034–5049.
- (30) Obermeyer, M.; Inhester, L.; Santra, R. Strategies for solving the excited-state self-consistent-field problem for highly excited and multiply ionized states. *Physical Review A* **2021**, *104*, 023115.
- (31) Carter-Fenk, K.; Herbert, J. M. State-targeted energy projection: A simple and robust

- approach to orbital relaxation of non-Aufbau self-consistent field solutions. *J. Chem. Theory Comput.* **2020**, *16*, 5067–5082.
- (32) Hait, D.; Head-Gordon, M. Excited state orbital optimization via minimizing the square of the gradient: General approach and application to singly and doubly excited states via density functional theory. *J. Chem. Theory Comput.* **2020**, *16*, 1699–1710.
- (33) Levi, G.; Ivanov, A. V.; Jónsson, H. Variational density functional calculations of excited states via direct optimization. *J. Chem. Theory Comput.* **2020**, *16*, 6968–6982.
- (34) Levi, G.; Ivanov, A. V.; Jónsson, H. Variational calculations of excited states via direct optimization of the orbitals in DFT. *Faraday Discussions* **2020**, *224*, 448–466.
- (35) Ivanov, A. V.; Jónsson, E.; Vegge, T.; Jónsson, H. Direct energy minimization based on exponential transformation in density functional calculations of finite and extended systems. *Computer Physics Communications* **2021**, *267*, 108047.
- (36) Head-Gordon, M.; Pople, J. A. Optimization of Wave Function and Geometry in the Finite Basis Hartree-Fock Method. *J. Phys. Chem* **1988**, *92*, 3063–3069.
- (37) Loos, P.-F.; Comin, M.; Blase, X.; Jacquemin, D. Reference energies for intramolecular charge-transfer excitations. *J. Chem. Theory Comput.* **2021**, *17*, 3666–3686.
- (38) Kozma, B.; Tajti, A.; Demoulin, B.; Izsák, R.; Nooijen, M.; Szalay, P. G. A new benchmark set for excitation energy of charge transfer states: systematic investigation of coupled cluster type methods. *J. Chem. Theory Comput.* **2020**, *16*, 4213–4225.
- (39) Zhao, Y.; Truhlar, D. G. Density functional for spectroscopy: No long-range self-interaction error, good performance for Rydberg and charge-transfer states, and better performance on average than B3LYP for ground states. *Journal of Physical Chemistry A* **2006**, *110*, 13126–13130.

- (40) Bogo, N.; Stein, C. J. Benchmarking DFT-based excited-state methods for intermolecular charge-transfer excitations. *Phys. Chem. Chem. Phys.* **2024**, *26*, 21575–21588.
- (41) Perdew, J. P.; Burke, K.; Ernzerhof, M. Generalized gradient approximation made simple. *Phys. Rev. Lett.* **1996**, *77*, 3865.
- (42) Blöchl, P. E. Projector augmented-wave method. *Phys. Rev. B* **1994**, *50*, 17953–17979.
- (43) Dunning, T. H. Gaussian basis sets for use in correlated molecular calculations. I. The atoms boron through neon and hydrogen. *J. Chem. Phys.* **1989**, *90*, 1007–1023.
- (44) Kendall, R. A.; Dunning, T. H.; Harrison, R. J. Electron affinities of the first-row atoms revisited. Systematic basis sets and wave functions. *J. Chem. Phys.* **1992**, *96*, 6796–6806.
- (45) Woon, D. E.; Dunning, T. H. Gaussian basis sets for use in correlated molecular calculations. IV. Calculation of static electrical response properties. *J. Chem. Phys.* **1994**, *100*, 2975–2988.
- (46) Rossi, T. P.; Lehtola, S.; Sakko, A.; Puska, M. J.; Nieminen, R. M. Nanoplasmonics simulations at the basis set limit through completeness-optimized, local numerical basis sets. *J. Chem. Phys.* **2015**, *142*, 094114.
- (47) Larsen, A. H.; Vanin, M.; Mortensen, J. J.; Thygesen, K. S.; Jacobsen, K. W. Localized atomic basis set in the projector augmented wave method. *Phys. Rev. B, Condens. Matter* **2009**, *80*, 195112.
- (48) Mortensen, J. J.; Larsen, A. H.; Kuisma, M.; Ivanov, A. V.; Taghizadeh, A.; Peterson, A.; Haldar, A.; Dohn, A. O.; Schäfer, C.; Jónsson, E. Ö.; Hermes, E. D.; Nilsson, F. A.; Kastlunger, G.; Levi, G.; Jónsson, H.; Häkkinen, H.; Fojt, J.; Kangsabanik, J.; Sødequist, J.; Lehtomäki, J.; Heske, J.; Enkovaara, J.; Winther, K. T.; Dulak, M.; Melander, M. M.; Ovesen, M.; Louhivuori, M.; Walter, M.; Gjerding, M.;

- Lopez-Acevedo, O.; Erhart, P.; Warmbier, R.; Würdemann, R.; Kaappa, S.; Latini, S.; Boland, T. M.; Bligaard, T.; Skovhus, T.; Susi, T.; Maxson, T.; Rossi, T.; Chen, X.; Schmerwitz, Y. L. A.; Schiøtz, J.; Olsen, T.; Jacobsen, K. W.; Thygesen, K. S. GPAW: open Python package for electronic-structure calculations. *Journal of Chemical Physics* **2024**, *160*, 092503.
- (49) Ziegler, T.; Rauk, A.; Baerends, E. J. On the calculation of multiplet energies by the Hartree-Fock-Slater method. *Theor. Chem. Acc.* **1977**, *43*, 261–271.
- (50) Le Bahers, T.; Adamo, C.; Ciofini, I. A qualitative index of spatial extent in charge-transfer excitations. *J. Chem. Theory Comput.* **2011**, *7*, 2498–2506.
- (51) Enkovaara, J.; Rostgaard, C.; Mortensen, J. J.; Chen, J.; Dułak, M.; Ferrighi, L.; Gavnholt, J.; Glinsvad, C.; Haikola, V.; Hansen, H.; others Electronic structure calculations with GPAW: a real-space implementation of the projector augmented-wave method. *J. Phys. Condens. Matter* **2010**, *22*, 253202.
- (52) Mortensen, J. J.; Hansen, L. B.; Jacobsen, K. W. Real-space grid implementation of the projector augmented wave method. *Phys. Rev. B* **2005**, *71*, 035109.
- (53) Neese, F. The ORCA program system. *Wiley Interdisciplinary Reviews: Computational Molecular Science* **2012**, *2*, 73–78.
- (54) Neese, F. Software update: The ORCA program system—Version 5.0. *Wiley Interdisciplinary Reviews: Computational Molecular Science* **2022**, *12*, e1606.
- (55) Hellgren, M.; Gross, E. K. Discontinuities of the exchange-correlation kernel and charge-transfer excitations in time-dependent density-functional theory. *Phys. Rev. A* **2012**, *85*, 022514.
- (56) Dreuw, A.; Head-Gordon, M. Failure of time-dependent density functional theory for

long-range charge-transfer excited states: the zincbacteriochlorin- bacteriochlorin and bacteriochlorophyll- spheroidene complexes. *J. Am. Chem. Soc.* **2004**, *126*, 4007–4016.

- (57) Dreuw, A.; Weisman, J. L.; Head-Gordon, M. Long-range charge-transfer excited states in time-dependent density functional theory require non-local exchange. *J. Chem. Phys.* **2003**, *119*, 2943–2946.

Supporting information for "Freeze-and-release direct optimization method for variational calculations of excited electronic states"

Yorick L. A. Schmerwitz,^{*,†,‡} Elli Selenius,[†] and Gianluca Levi^{*,†}

[†]*Science Institute of the University of Iceland, Reykjavík, Iceland*

[‡]*Max-Planck-Institut für Kohlenforschung, 45470 Mülheim an der Ruhr, Germany*

E-mail: schmerwitz@kofo.mpg.de; giale@hi.is

Table S1: Excitation energy (in eV) of charge transfer states of organic molecules obtained from orbital optimized calculations using DO and TD-DFT calculations with local and semi-local functionals, together with the mean absolute and mean signed errors (MAE and MSE) with respect to theoretical best estimate (TBE) values.¹ The charge transfer distance (in Å), d^{CT} , of the orbital optimized spin-mixed excited state solution obtained with PBE is also shown together with the electronic distance, η , of this solution from the initial guess.

Molecule	Sym.	TBE ^a	FR-DO		DO-MOM		SCF-MOM	
		ΔE	ΔE	d_{CT}	ΔE	d_{CT}	ΔE	d_{CT}
Aminobenzonitrile (ABN)	A ₁	5.09	3.69	1.06	3.69	1.06	3.69	1.06
Aniline	A ₁	5.48	4.31	0.82	4.31	0.82	4.31	0.82
Azulene	A ₁	3.84	3.00	0.94	3.00	0.94	3.00	0.94
	B ₂	4.49	3.97	0.77	3.97	0.77	3.97	0.77
Benzothiadiazole (BTD)	B ₂	4.28	3.08	1.19	3.08	1.19	3.08	1.19
Benzonitrile	A ₂	7.05	6.57	1.04	5.96	0.58	-	-
Dimethylaminobenzonitrile (DMABN)	A ₁	4.86	3.53	1.55	3.53	1.56	3.54	1.56
Twisted DMABN	A ₂	4.12	3.56	2.04	3.56	2.04	3.56	2.05
	B ₁	4.75	4.21	1.75	4.21	1.75	4.21	1.75
Dimethylaniline (DMAn)	A ₁	5.40	4.17	1.33	4.17	1.33	4.18	1.33
	B ₂	4.40	3.82	1.08	3.82	1.08	3.82	1.08
Hydrogen Chloride	II	7.88	7.33	0.86	7.33	0.86	7.33	0.86
Nitrodimethylaniline (NDMA)	A ₁	4.39	3.05	2.34	3.05	2.34	3.05	2.34
Nitropyridine <i>N</i> -Oxide (NPNO)	A ₁	5.39	2.73	1.72	2.73	1.72	2.73	1.72
p-Nitroaniline	A ₁	4.13	3.26	2.05	3.26	2.05	3.26	2.05
Nitrobenzene	A ₁	4.10	4.13	1.46	4.13	1.46	4.13	1.47
<i>N</i> -Phenylpyrrole (PP)	A ₁	5.86	5.14	2.02	4.69	1.85	5.14	2.03
	B ₂	5.32	4.12	1.59	4.12	1.59	-	-
Twisted PP	A ₁	5.65	5.56	2.41	4.61	2.06	5.56	2.41
	A ₂	5.95	5.40	2.15	5.40	2.15	5.40	2.15
	B ₁	6.17	5.42	2.16	5.42	2.16	5.42	2.16
	B ₂	5.58	5.26	2.36	4.58	2.04	5.27	1.49
Phthalazine	A ₂	3.91	3.10	1.26	3.10	1.26	3.11	1.26
	B ₁	4.31	3.45	1.26	3.45	1.26	3.45	1.26
Quinoxaline	A ₁	5.65	4.56	0.62	4.56	0.62	4.56	0.62
	B ₁	6.22	5.15	1.24	5.15	1.24	5.15	1.24
	B ₂	4.63	3.48	1.25	3.48	1.25	3.48	1.25

^a Theoretical best estimates obtained at the CCSDT/aug-cc-pVQZ level in ref. 1

Table S2: Estimation of the saddle point order of spin-mixed charge transfer excited state solutions of organic molecules. The calculations use the PBE functional and the aug-cc-pVDZ+sz basis set. The values in parentheses are the number of negative eigenvalues with an absolute value bigger than 1 eV. Constrained minimization leads to a significant improvement in the estimated saddle point order for both a numerical eigendecomposition of the Hessian and a diagonal analytic approximation (preconditioner of eq. 7).

Molecule	Sym.	Initial guess		Constrained solution		Final solution
		Num. Hessian	Precond. (eq. 7)	Num. Hessian	Precond. (eq. 7)	Num. Hessian
Aminobenzonitrile (ABN)	A ₁	2 (1)	1	1 (1)	1	1
Aniline	A ₁	4 (2)	3	3 (1)	3	3
Azulene	A ₁	2 (2)	2	2 (2)	2	2
	B ₂	3 (3)	3	3 (3)	3	3
Benzothiadiazole (BTD)	B ₂	4 (3)	1	1 (1)	1	1
Benzonitrile	A ₂	14 (13)	3	6 (6)	6	6
Dimethylaminobenzonitrile (DMABN)	A ₁	4 (1)	1	1 (1)	1	1
Twisted DMABN	A ₂	22 (18)	1	6 (3)	6	3
	B ₁	25 (22)	2	5 (5)	5	5
Dimethylaniline (DMA)	A ₁	8 (4)	3	4 (2)	3	3
	B ₂	11 (8)	1	2 (1)	2	2
Hydrogen Chloride	Π	2 (1)	1	2 (1)	1	1
Nitrodimethylaniline (NDMA)	A ₁	41 (26)	1	6 (4)	5	3
Nitropyridine <i>N</i> -Oxide (NPNO)	A ₁	13 (9)	1	4 (3)	4	2
Nitroaniline	A ₁	31 (19)	1	5 (4)	5	3
Nitrobenzene	A ₁	18 (14)	3	5 (4)	5	4
<i>N</i> -Phenylpyrrole (PP)	A ₁	43 (36)	2	9 (6)	9	5
	B ₂	13 (8)	1	3 (3)	3	2
Twisted PP	A ₁	42 (35)	2	12 (7)	11	11
	A ₂	38 (29)	2	11 (7)	11	7
	B ₁	38 (34)	3	12 (7)	12	6
	B ₂	38 (31)	1	10 (6)	10	9
Phthalazine	A ₂	14 (12)	1	2 (1)	2	2
	B ₁	11 (8)	2	3 (1)	3	2
Quinoxaline	A ₁	5 (5)	3	3 (3)	3	3
	B ₁	10 (9)	3	4 (4)	4	4
	B ₂	6 (4)	2	4 (2)	4	2
Avg. abs. deviation		13.6 (9.7)	1.7	1.22 (0.7)	1.07	0
Max. abs. deviation		38 (31)	9	6 (4)	6	0

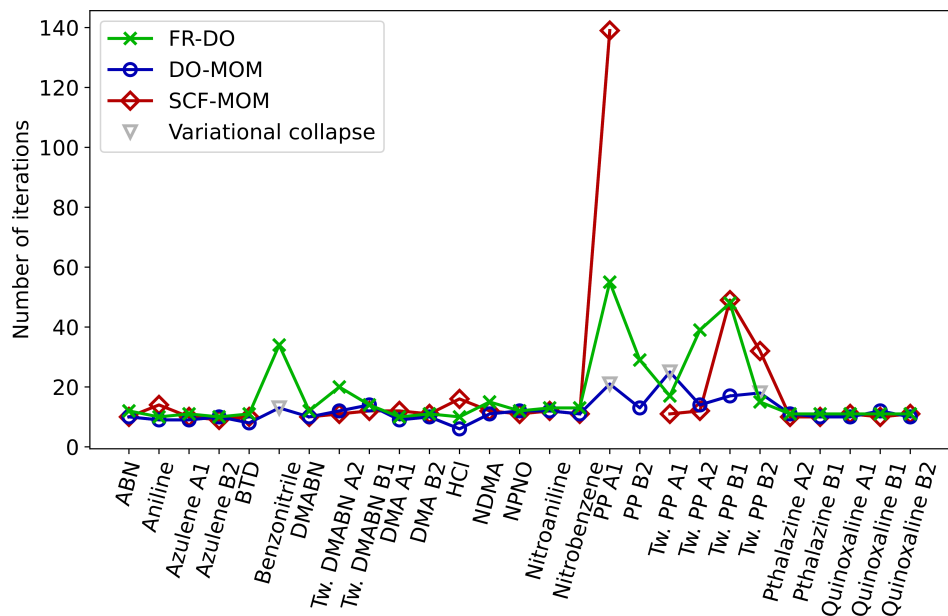


Figure S1: Numbers of iterations taken by freeze-and-release direct optimization (FR-DO, green crosses), direct optimization with the maximum overlap method (DO-MOM, blue circles), and self-consistent field with the maximum overlap method (SCF-MOM, red diamonds) to converge each excited state in the set of intramolecular charge transfer states. Variational collapses are indicated by gray triangles.

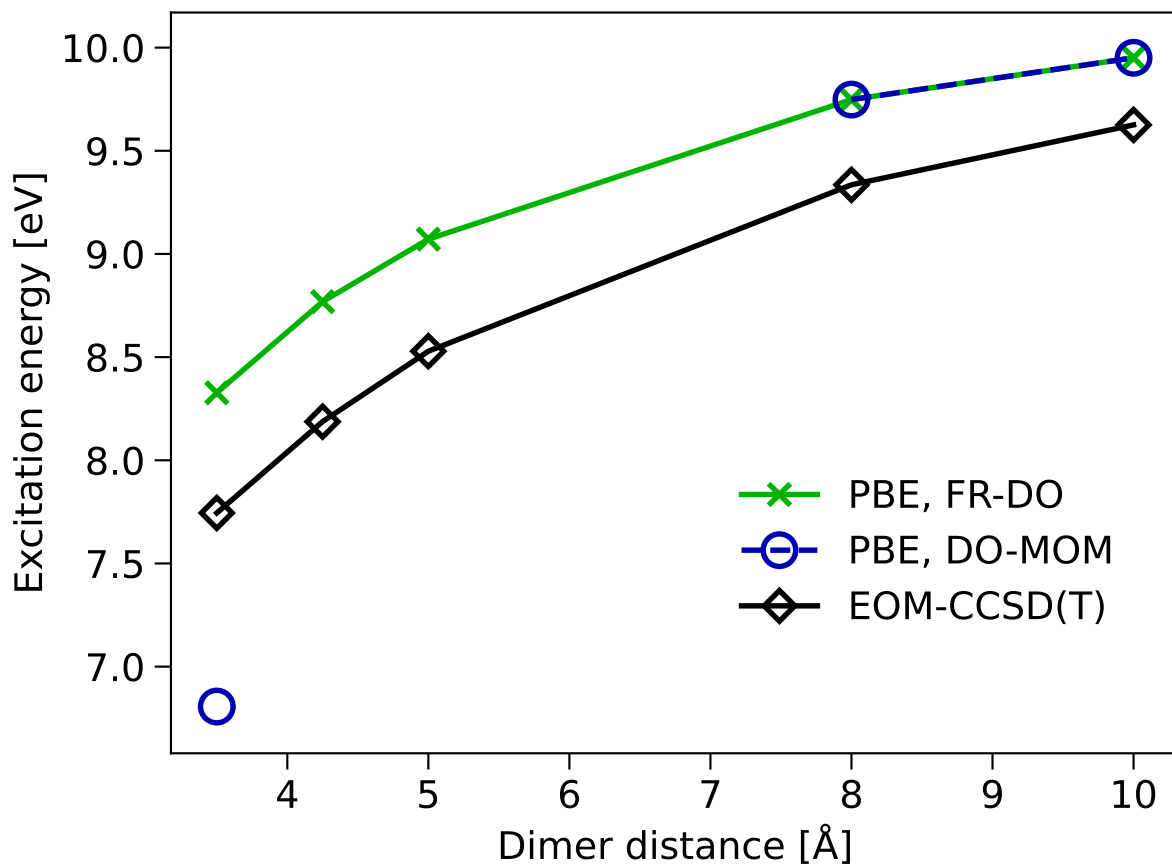


Figure S2: Comparisons of the excitation energy of the ammonia-difluorine dimer depending on the distance between the molecular fragments obtained with FR-DO (green crosses) and DO-MOM (blue circles) with the PBE functional and the aug-cc-pVDZ basis set, and taken from published EOM-CCSD(T) calculations² (black squares). The FR-DO excitation energy curve agrees well with the many-body results. DO-MOM shows a variational collapse at a dimer distance of 3.5 Å and otherwise does not converge within 333 iterations until a distance of 8 Å is reached, above which it converges to the same solution as FR-DO.

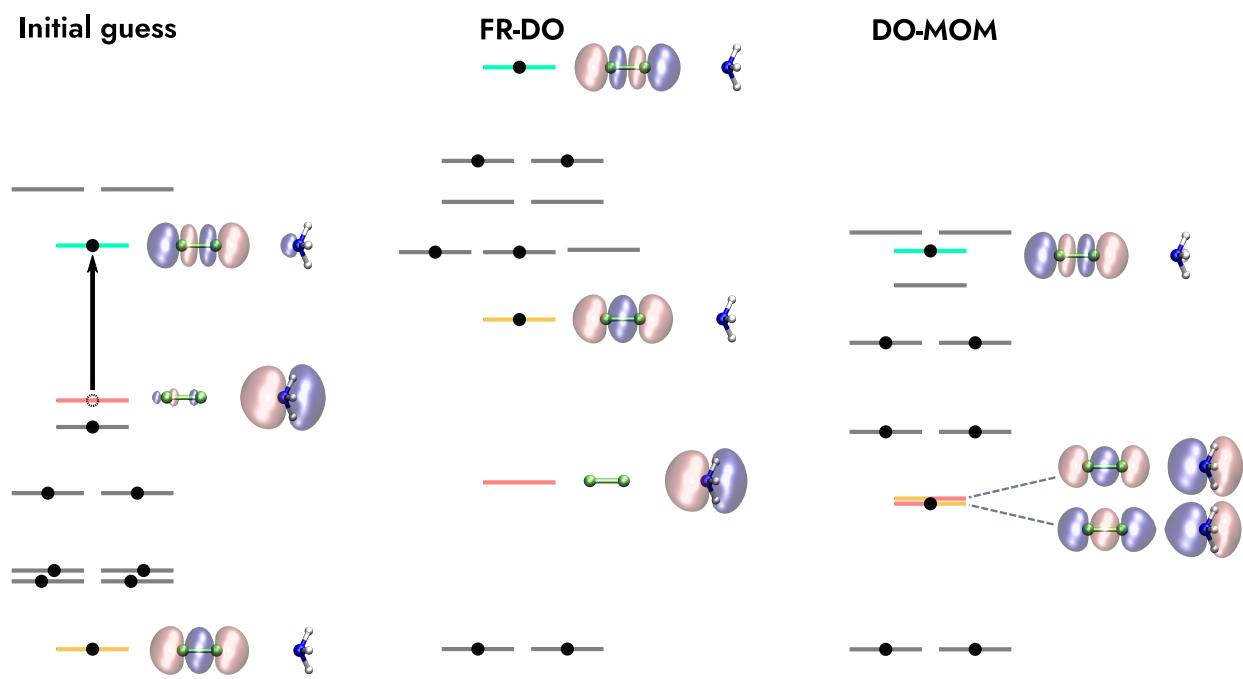


Figure S3: The relevant MOs of the initial guess, the FR-DO solution, and the DO-MOM solution for ammonia-difluorine at a separation of 3.5 Å. The orbitals are visualized with isosurface values of $\pm 0.08 \text{ \AA}^{-3}$.

References

- (1) Loos, P.-F.; Comin, M.; Blase, X.; Jacquemin, D. Reference energies for intramolecular charge-transfer excitations. *Journal of Chemical Theory and Computation* **2021**, *17*, 3666–3686.
- (2) Bogo, N.; Stein, C. J. Benchmarking DFT-based excited-state methods for intermolecular charge-transfer excitations. *Phys. Chem. Chem. Phys.* **2024**, *26*, 21575–21588.